Geol. Mag. **144** (*4*), *2007, pp. 731–739.* © *2007 Cambridge University Press*

doi:10.1017/S0016756807003457 First published online 20 April 2007 *Printed in the United Kingdom*

Amethyst geodes in the basaltic flow from Triz quarry at Ametista do Sul (Rio Grande do Sul, Brazil): magmatic source of silica for the amethyst crystallizations

DOMINIQUE PROUST* & CLAUDE FONTAINE

UMR 6532 CNRS, HydrASA, Faculté des Sciences, 40 Avenue du recteur Pineau, 86022 Poitiers cedex, France

(*Received* 21 March 2006; *accepted* 14 August 2006)

Abstract – The amethyst geodes observed in the tholeiitic basaltic flow from the Triz quarry at Ametista do Sul (Rio Grande do Sul, Brazil) show particular wall-layering infillings with, from the outside inwards, celadonite, chalcedony, fine-grained quartz and large-sized amethyst crystals. The primary fluid inclusions analysed in the amethyst crystals yield a 152 to 238 °C crystallization temperature range. The amethyst geodes are always located in the massive, fracture-free, basaltic part of the lava flows and surrounded by a limited wall-lining alteration halo, the thickness of which depends on the geode radius. The geochemical balances calculated from fresh to altered basalt in the geode environment indicate that the amount of SiO_2 released from the alteration halo is always sufficient to produce the siliceous rims in the geodes without requirement for extraneous silica supply. The results point to a volcanic origin for the amethyst geode infillings through basalt 'autoalteration' by authigenic high temperature hydrothermal fluids. These fluids can originate from (1) unmixing of volatile coumpounds from melt through pressure release, (2) cooling to supercritical hydrous fluids with 'autoalteration' of the surrounding basalt and (3) migration of the residual hot fluids from the basalt to the geodic cavities through the pressure gradient between the geodic cavity and the rock.

Keywords: basaltic flows, geodes, amethyst, geochemical profiles, fluid inclusions.

1. Introduction

The thick basaltic flows in southern Brazil, Uruguay and Argentina are famous for their large-sized amethyst geodes, which are always located in the upper third of the flows. These amethyst geodes result from two successive physicochemical processes: (1) the formation of the geodic cavity by degassing of the magma due to pressure release with the nucleation, growth and coalescence of bubbles and (2) the geode infilling by siliceous crystallizations. Bubble formation by magmatic degassing and coalescence is considered to be the primary mechanism for formation of large geodic cavities in lavas (Gilg *et al.* 2003; Proust & Fontaine, 2007). Two main hypotheses, based on fluid inclusion and stable isotope data, are proposed to explain the geode filling processes from these pre-existing cavities or 'protogeodes': (1) Gilg *et al.* (2003), without completely excluding a magmatic source, suggest that the fluids could be meteoric water ascending from the artesian Botucatu aquifer sytem and that the silica source results from the interaction between the highly reactive basaltic glass and this ascending fluid with low salinity (< 2 wt % NaCl) and temperatures never exceeding 100 °C. (2) Other authors suggest that the silica source for geode infilling is the result of alteration of the enclosing basaltic rock by residual post-magmatic (Flörke, 1972; Flörke *et al.* 1982) or hydrothermal fluids (Sunagawa & Ohta, 1976; Meunier *et al.* 1988; Duarte, Hartmann & Vasconcellos, 2005). In a different way, Bossi & Caggiano (1974), Borget (1985) and Montana & Bossi (1993) proposed the fusion or dissolution of sandstones relics for the source of silica. Finally, Wang & Merino (1990) and Merino, Wang & Deloule (1995) proposed a model for agate crystallization from a silica-rich lump already accumulated in geodic space but did not choose between water–rock interaction and liquid immiscibility as the primary process.

The present study focused on one amethyst-bearing tholeiitic basaltic flow from Ametista do Sul (Brazil) in order to investigate, from fluid inclusion and geochemical mass balance studies, the temperature conditions and the possible silica origin for the amethyst crystallizations. This work developed in two stages: (1) the study of the mineralogical and chemical zonation in the geodic infillings and (2) the study of the chemical evolution of the host basalt in the geode environment.

2. The basaltic flow

The studied amethyst-bearing basaltic flow (Ametista do Sul, Brazil) was previously described in Proust & Fontaine (2007). It belongs to the Serra Geral Formation, a volcanic pile of 12 nearly horizontal flow units

*Author for correspondence: dominique.proust@univ-poitiers.fr

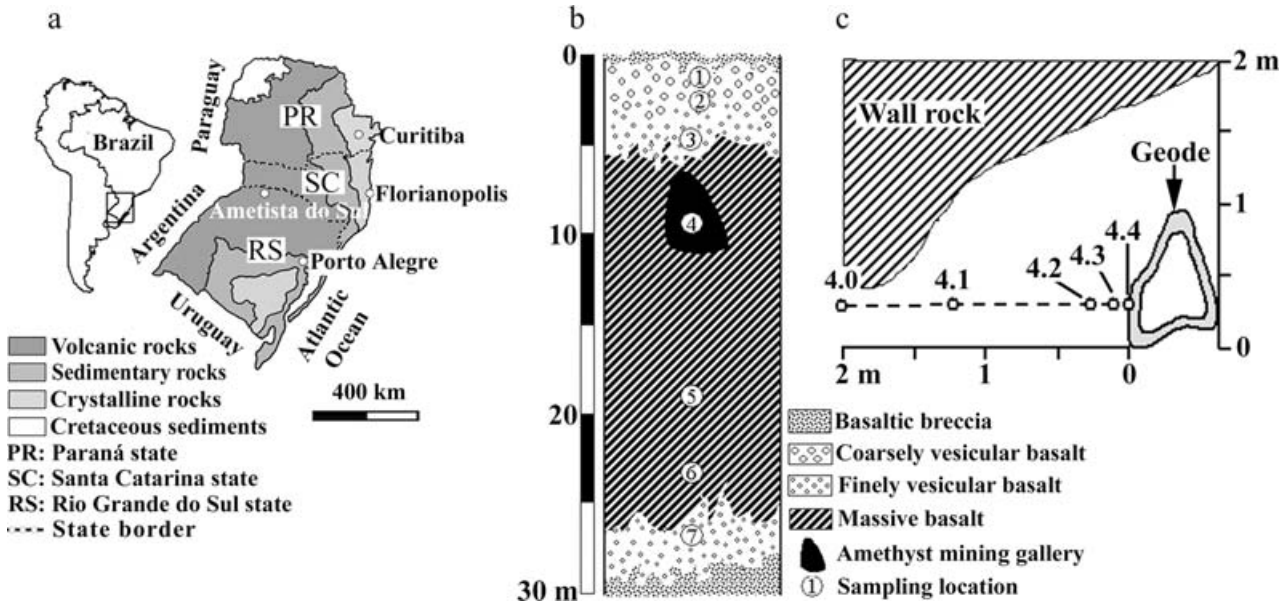

Figure 1. Geological setting and geode-bearing lava flow: (a) geographical and geological settings of the Paraná basin; (b) vertical cross-section of the lava flow in Triz quarry; 1, 2. . .7: sampling locations; (c) horizontal sampling along the amethyst level from the basalt to the edge of the geode; 4.0, 4.1. . .4.4: sampling locations.

in which four are amethyst-mineralized (Gomes *et al.* 2005). The studied basaltic flow is 30 m thick and crops out at the Triz quarry working-face (27°21′38.42″ S, 53°09′37.84″ W), east of Ametista do Sul (Fig. 1a). It belongs to the type I lava flow described by Long & Wood (1986) on the basis of its internal structure (Fig. 1b): on a vertical profile, the lava flow appears intercalated between two beds of reddish breccias, 1 m thick with sandstone blocks. No prismatic jointing is apparent at the outcrop, but one observes a massive, vesicle-free central part, about 20 m thick, sandwiched between two greenish-brown vesicular zones. The upper vesicular zone is 5 m thick and grades upward from finely vesicular basalt with millimetric vesicles to coarsely vesicular basalt with centimetric vesicles in contact with flow-top breccias. The lower vesicular zone is 2 m thick and entirely made up of finely vesicular basalt. The level of amethyst geodes is less than 3 m thick, and the contact between the host massive basalt and the geodes is always rimmed with a few millimetres of green clay. Five galleries, mining amethyst in the same geodic level, were investigated in the studied lava flow. All geodes observed in the five galleries displayed the same organization, considering the distance between two successive cavities, their shape and their infillings (nature and distribution of crystallizations). The same relationships between the geode radius and the silica rim thickness were observed and studied using image analysis from 106 exposed amethyst geodes. The image analysis of these amethyst geodes gives a maximum radius of 53.30 cm with a maximum silica rim thickness of 11.30 cm, that is, a maximum geode infilling of 49 %.These observations contributed to selection of a representative mining site which was sampled in the infilling materials, and respectively at 0, 8, 20, 120, 200 cm from the edge of the geode into the host basalt (Fig. 1c, Table 1).

3. Analytical methods

The petrographical and mineralogical investigations of the amethyst-bearing level were performed on diamond-polished thin-sections using a CAMECA SX 50 electron microprobe (W.D.S. analysis) at the 'Service d'analyse CAMPARIS', University of Paris VI. The analytical conditions were: accelerating voltage of 15 kV, beam spot-size of 1 μm, beam current of 4 nA, counting time of 10 s for each analysed element. The results of Electron Probe MicroAnalyses (EPMA) were plotted into the M^{+}–4Si–$3R^{2+}$ chemiographic representation, which discriminates the major dioctahedral and trioctahedral clay minerals into well-separated chemical domains. The chemiographic poles were calculated on the basis of cations per formula unit as: $M^{+} = 2Ca^{2+} + Na^{+} + K^{+}$, $4Si = Si^{4+}/4$ and $3R^{2+} = (Fe^{2+} + Mg^{2+} + Mn^{2+})/3$; for direct chemical compositions, whole minerals (including celadonites) were plotted with total iron expressed as Fe^{2+} atoms. Mineral identifications were completed by X-ray diffraction (XRD) on random powders and Ca-saturated oriented preparations using a PHILIPS PW 1730 diffractometer (40 kV, 40 mA) with Fe-filtered Co$K\alpha$ radiation. The X-ray diffractograms were recorded using a stepping motor-driven goniometer with a DACO-MP recorder using the DIFFRAC AT software (SOCABIM). XRD patterns were then decomposed into their elementary components using the DECOMPXR decomposition program (Lanson & Besson, 1992).

https://doi.org/10.1017/S0016756807003457 Published online by Cambridge University Press

Table 1. Bulk chemical analyses (wt %) and apparent densities (g/cm^3) of sampled rocks

	Vertical sampling (Fig. 1b)							Horizontal sampling (Fig. 1c)				
Samples*	1	2	3	4	5	6	7	4.0	4.1	4.2	4.3	4.4
SiO_2	47.00	47.80	46.40	51.80	51.40	49.80	47.30	51.80	48.60	50.00	48.40	47.76
Al_2O_3	13.40	13.00	12.20	12.70	12.60	12.40	13.10	12.70	13.10	13.20	12.80	13.20
FeO**	15.32	14.59	14.50	13.51	14.37	14.23	14.86	13.51	14.71	14.85	14.88	14.76
MgO	4.60	4.15	5.10	4.90	4.80	4.50	4.30	4.90	4.76	4.30	4.50	4.76
MnO	0.25	0.25	0.20	0.20	0.25	0.15	0.20	0.20	0.25	0.20	0.22	0.26
TiO_2	3.30	3.10	3.30	3.20	2.80	3.40	3.15	3.20	3.90	3.60	3.90	3.78
CaO	6.80	6.90	7.60	7.30	6.40	7.60	7.10	7.30	8.10	7.60	7.50	8.18
Na_2O	2.30	2.30	2.00	2.50	2.15	2.45	2.20	2.50	2.60	2.80	2.48	2.55
K_2O	1.30	1.50	0.80	1.70	1.45	1.40	1.20	1.70	1.03	1.60	1.70	0.88
L.O.I.	4.30	5.30	6.30	2.10	1.85	1.70	4.60	2.10	2.70	1.50	1.95	3.00
Density	2.72	2.55	2.67	2.89	2.86	2.91	2.62	2.89	2.81	2.83	2.76	2.72

*Numbers refer to Figure 1b, c; **Total iron expressed as FeO. L.O.I. – Loss On Ignition.

The microthermometric measurements were performed on the fluid inclusions observed in the amethyst crystals of one geodic cavity using a CHAIXMECA heating–freezing (liquid nitrogen) microscope stage.

In order to calculate geochemical mass balances, chemical analyses of the bulk samples were performed by flame atomic absorption spectroscopy using a PERKIN ELMER 2380 instrument, whereas apparent densities were obtained by the hydrostatic balance method; the measurements were recorded from paraffin-coated, vesicle-free parts of the samples in order to establish coherent chemical comparisons between the massive and vesicular basalt. The bulk chemistry and the apparent density of each sample are given in Table 1.

The diameters of the geodic cavities and their silica rim thicknesses in the five studied galleries and in the 106 exposed amethyst geodes were measured on photographs using a Macintosh-based image analysis system (Optiscan© and Optilab© software). The two-dimensional data were converted to three-dimensional values using the methods of Cashman & Marsh (1988).

4. Results

4.a. Petrography and mineralogy of the amethyst geode infillings

The macroscopic, microscopic and X-ray diffraction studies of one representative quartz geode sampled in the mining galleries show (Fig. 2a), from the host basalt (B) to the centre of the geode, four distinct mineralogical rims: (G1) a thin, millimetric external rim with green clay mineral crystallizations, (G2) a milky-white coloured rim, 5 to 10 mm wide, with intercalations of calcite, microcrystalline quartz, chalcedony and beige to yellow clay mineral patches, (G3) a wider rim (2 cm thick) of dark grey chalcedony, and (G4) an internal zone with a first centimetric rim of colourless quartz

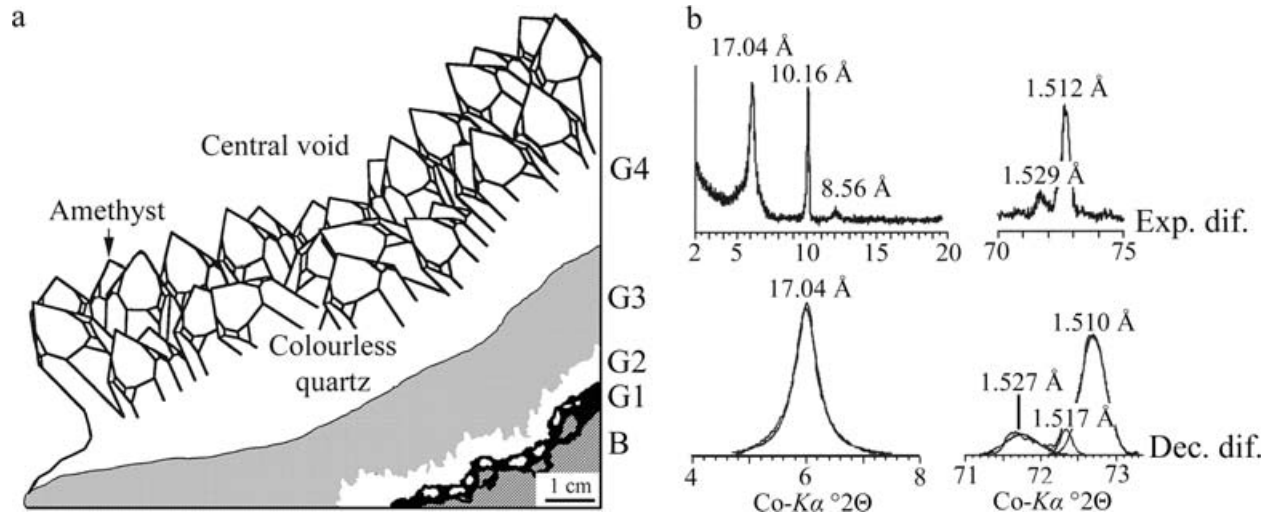

Figure 2. (a) Mineralogical organization of the geode infillings: (B) massive host basalt; (G1) green clay mineral external rim; (G2) milky-white coloured rim with calcite, microcrystalline quartz, chalcedony and beige to yellow clay mineral patches; (G3) dark grey chalcedony; (G4) quartz and amethyst crystallizations. (b) Experimental (Exp. dif.) and decomposed X-ray diffractograms (Dec. dif.) of the clay minerals microsampled from G1 and G2 rims of amethyst geode infillings.

https://doi.org/10.1017/S0016756807003457 Published online by Cambridge University Press

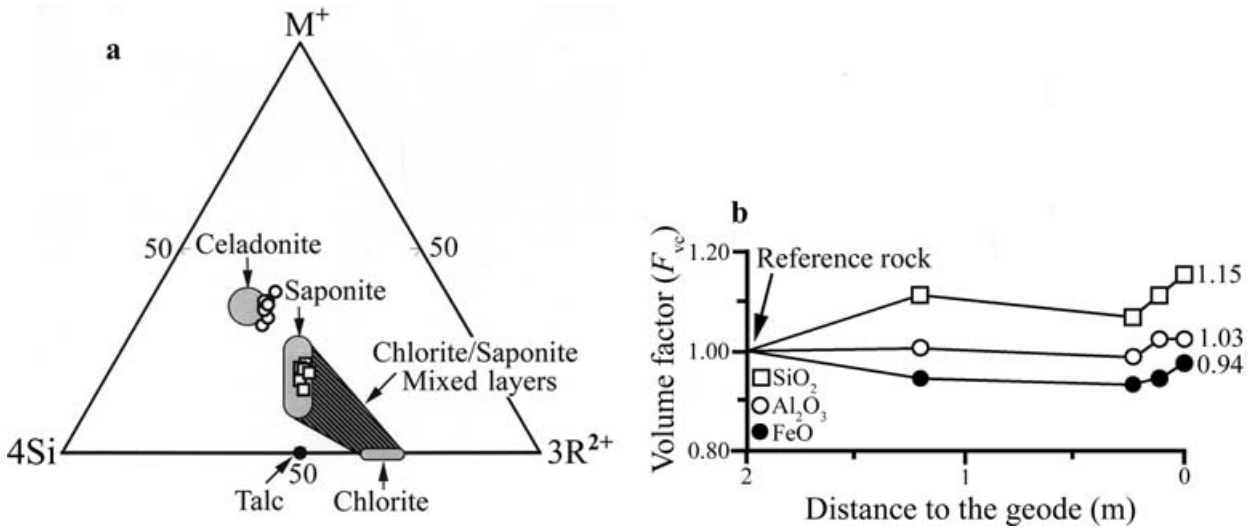

Figure 3. (a) Electron Probe MicroAnalyses of the clay minerals in geode infillings (cf. Fig. 2) as they plot onto the M^+–4Si–$3R^{2+}$ ternary diagram. Open circles: green celadonite spherulites in external rim; open squares: beige to yellow saponites in internal rim. (b) Determination and variation of the factor volume (F_{vc}) needed for $X_n = 0$ in horizontal flow cross-section: plots of F_{vc} calculated for SiO_2, Al_2O_3 and FeO oxides as a function of the distance to the geode.

grading into pluri-centimetric amethyst crystals. This general crystallization sequence of siliceous phases, from milky to grey chalcedony and amethyst, is indicative of increasing SiO_2/H_2O ratio as observed by Graetsch, Flörke & Miehe (1985). The experimental XRD patterns recorded from the clay minerals microsampled from the two most (G1 and G2) external rims (Fig. 2b) characterize, after ethylene-glycol solvation, a mixture of a smectite with (001) and (002) basal reflections at 17.04 Å and 8.56 Å, respectively, and a dioctahedral mica with a sharp (001) basal reflection at 10.16 Å. The decomposition of the (001) smectite reflection yields a unique component centred at 17.04 Å, whereas the (06,33) band decomposition is more complex with three components centred at 1.527, 1.517, and 1.510 Å. These three components can be respectively assigned to two smectite species, saponite and a minor amount of nontronite, and celadonite mica. The EPMA values (Table 2), when plotted into the M^+–4Si–$3R^{2+}$ ternary diagram, support the identification of the major clay minerals (Fig. 3a). The green outermost rim (G1) is high in silicon, iron and potassium and plots in the celadonite domain, whereas the beige to yellow clay mineral patches associated with calcite, quartz and chalcedony in the G2 rim are lower in silicon, iron and potassium and higher in magnesium and plot in the saponite domain. The celadonite of the G1 rim appears to form a coating around the geodic cavities which favours their extraction from the host basalt. On the other hand, it was also observed in basalt fragments forming breccias cemented by agate (Gilg *et al.* 2003). In agreement with these authors, such observations lead us to consider the celadonite as an alteration product of the host basalt.

Table 2. EPMA (wt %) and structural formulae of clay minerals lining the amethyst quartz geodes in massive basalt

	Outer rim G1 (n = 15)		Inner rim G2 (n = 7)	
	Mean	SD	Mean	SD
SiO_2	53.23	3.69	49.31	0.98
Al_2O_3	1.27	0.35	5.79	0.25
FeO*	21.60	1.33	18.31	0.72
MgO	5.02	0.45	10.27	0.61
TiO_2	0.07	0.05	0.14	0.10
MnO	0.02	0.05	0.00	0.00
CaO	0.22	0.20	1.69	0.18
Na_2O	0.12	0.24	0.10	0.05
K_2O	8.80	1.16	1.04	0.47
Total	90.37	–	86.66	–
Atoms on the basis of 11 oxygens				
Si	4.17	0.05	3.81	0.04
Al	0.12	0.04	0.53	0.02
Fe^{2+}	1.42	0.06	1.18	0.03
Mg	0.59	0.04	1.18	0.05
Ti	0.00	0.00	0.01	0.01
Mn	0.00	0.00	0.00	0.00
Ca	0.02	0.02	0.14	0.01
Na	0.02	0.05	0.02	0.01
K	0.88	0.09	0.10	0.05

*total iron as FeO; n – number of analyses; SD – standard deviation.

4.b. Microthermometric measurements

The studied fluid inclusions were located only in the amethyst crystals. These inclusions always contained two fluid-phases (vapour + liquid). The melting temperature ranges between −0.5 °C and −2.2 °C with a mean value of −1.5 °C, which characterizes very low saline fluids containing 1.40 eq. wt % NaCl (Potter, Clynne & Brown, 1978). The homogenization temperatures are much more scattered, ranging from

https://doi.org/10.1017/S0016756807003457 Published online by Cambridge University Press

152 °C to 238 °C. This wide variation in range can be correlated to the variations in the inclusion sizes and occurrences within the amethyst crystals. The highest homogenization temperatures (204 °C to 238 °C) are recorded in large (22 to 68 μm) tubular inclusions within healed fractures in the growth zones of the amethyst crystals. These fractures do not progress in the adjacent crystals and, according to Roedder (1981, 1984), these fluid inclusions can be termed primary, preserving the original fluids and their trapping conditions. The most abundant fluid inclusions occur as clusters of smaller inclusions (< 10 μm) along the boundary planes of the fractured crystals, yielding a lower homogenization temperature range (152 °C to 200 °C). They can be termed secondary inclusions, preserving post-crystallization fluid trapping conditions (Roedder, 1981). Since calculated homogenization temperatures correspond to the isochore minima along the liquid–vapour (H_2O) curve in the considered system, these temperatures need to be corrected as a function of the internal pressure in the geode cavity using the Laplace equation (Toramaru, 1995):

$$P_g - P_m = 2\gamma/R \qquad (1)$$

where P_g and P_m are the pressures (Pa) of H_2O vapour and silicate melt, respectively, γ is the interfacial tension (N/m) at the gas–magma interface and R is the bubble radius (m). The calculation for the geodes in the amethyst levels with the interfacial tensions ranging from 0.1 to 1.3 N/m (Taniguchi, 1988; Toramaru, 1989) yields maximum internal pressure of water vapour ranging from 2.55 to 2.61×10^5 Pa. Roedder (1984) demonstrated that these low pressure conditions, together with the low fluid salinity, define a homogenization temperature correction which is far below the measurement uncertainty of ± 10 °C. When primary fluid inclusions are concerned, the measured homogenization temperatures (204 °C to 238 °C) are in good agreement with the fluid inclusion data obtained by Balitsky (1978), Robinson & Norman (1984) and Gatter (1987) in epithermal amethyst deposits hosted by volcanic rocks. In contrast, the secondary fluid inclusions which are the most abundant in amethyst crystals yield a lower homogenization temperature range (152 °C to 200 °C), closer to the data obtained by Fallick *et al.* (1985), Fallick, Jocelyn & Hamilton (1987), and Harris (1989), using stable oxygen isotopes from amethyst and agate geodes (< 150 °C). The importance of the secondary fluid inclusions relative to the primary ones could explain the lower values obtained by bulk isotopic analyses.

4.c. Geochemical mass balances

The Paraná tholeiitic basalts are divided into high-TiO_2 (northern Paraná basin) and low-TiO_2 basalts (southern Paraná basin) with a separating line at 2 wt % TiO_2 (Bellieni *et al.* 1984). The massive basalt from the Triz flow belongs to the high-TiO_2 group with TiO_2 contents ranging from 2.80 to 3.40 wt % (samples 4, 5 and 6 in Table 1). They are mainly distinguished from the upper and lower vesicular levels by higher SiO_2 (mean: +3.9 %), lower H_2O (L.O.I.) contents (mean: −3.2 %) and higher apparent densities (mean: +0.25). The variations of the other major elements remain in the range of the analysis error (SiO_2 ± 1.0 wt %; Al_2O_3 and TiO_2 ± 0.5 wt %; FeO ± 0.2 wt %) and cannot be considered as indicating a chemical differentiation. A review of the numerous chemical analyses achieved on the Paraná basalts (Peate, Hawkesworth & Mantovani, 1992) gives 2.5 wt % as the upper limit for H_2O content in unaltered high-TiO_2 basalts and 50.20 to 52.00 wt % as the SiO_2 content range. All massive basalt samples meet the H_2O content condition, which is indicative of low secondary hydrous mineral contents. On the other hand, if sample 6 is out of the SiO_2 range, sample 4, with the highest SiO_2 content (51.80 wt %) and higher apparent density than sample 5, will serve as reference (least altered) sample for the geochemical mass balance calculation. The chemical compositions and the apparent densities of the rocks horizontally sampled along the amethyst mining gallery (samples 4.0 to 4.4 in Table 1) show significant variations with the decreasing distance to the geode: (1) the progressive decrease in the SiO_2 contents and apparent densities, and (2) the slight increase in the water contents which account for a progressive increase in the rock alteration with subsequent SiO_2 release towards the contact with the geode.

Many mass-balance models have been published in the literature to investigate and quantify the changes in rock chemical and physical properties induced by its interaction with fluids. These models cover a wide range of geochemical environments such as alteration, diagenesis, metamorphism and magmatism (Gresens, 1967; Albarede & Provost, 1977; Grant, 1986; Brimhall & Dietrich, 1987; MacLean, 1990; Potdevin, 1993; Biddle, Chittleborough & Fitzpatrick, 1998; Sturm 2003). Most of these models are based upon the general equation of Gresens (1967), where bulk densities and chemical data of altered rocks are compared to those of a reference rock in order to quantify the losses or gains of elements resulting from rock–fluid interactions:

$$X_n = \{F_v(da_x/da_y)C_x\} - C_y \qquad (2)$$

where X_n is the amount (g) of the oxide n gained ($X_n > 0$) or lost ($X_n < 0$) per 100 grams of rock, F_v is the volume factor, da_x and da_y are the apparent densities, C_x and C_y are the concentrations of the oxide n (wt %) of the reference and altered rocks, respectively. Geochemical mass balances can be calculated using either rock volume or the concentration of a given element as invariant. Rock alteration usually induces an increase in volume, and mass balances are thus

https://doi.org/10.1017/S0016756807003457 Published online by Cambridge University Press

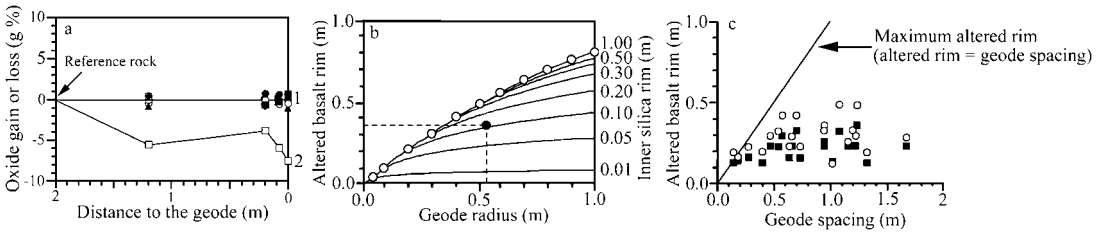

Figure 4. (a) Geochemical mass balance (g per 100 g of rock) calculated along the horizontal flow cross-section; (1) invariant behaviour of all oxides except SiO_2; (2) SiO_2 loss (open squares). Symbols as in Figure 3b. (b) Estimation of the altered basalt rim surrounding the geodes as a function of geode radii and inner silica rims; open circles: altered basalt rims for geodes with 100 % silica infilling; filled circle: altered basalt rim for the 'maximum' geode with 53.30 cm radius and 11.30 cm silica rim. (c) Plots of the altered basalt rim surrounding the geodes in the mining galleries as a function of their spacing; altered basalt rims were calculated for 100 % geode infilling (open circles) and 49 % geode infilling (black squares).

currently calculated using Al_2O_3 or TiO_2 as invariant. In this case, a volume factor required for a given oxide n to be constant during alteration (F_{vc}) can be calculated setting $X_n = 0$ in equation (2) for the most abundant major elements, that is, SiO_2, Al_2O_3 and FeO in horizontally sampled rocks (Fig. 3b). The F_{vc} values for SiO_2 range from 1 in the reference sample to 1.15 at the contact with the geode, whereas F_{vc} for Al_2O_3 and FeO are almost constant (0.94 and 1.03). Therefore, the most appropriate method for the following mass transfer calculation was to use $F_{vc} = 1$ in order to correlate the element gain or loss as a function of the distance to the geode. The model proceeds by incrementation of the 100 cm^3 elementary volume. Apart from SiO_2, which is the only mobile element with a mass release of up to 7.53 g per 100 g at the contact with the geode, the major elements do not show any significant mass release from rock to geode (Fig. 4a).

5. Discussion

The formation of the geodic cavities (protogeodes) during the lava flow degassing process is related to the growth and coalescence of bubbles (Proust & Fontaine, 2007), which are predominantly filled with water vapour and CO_2 (Anderson, 1975; Sparks, 1978; Toramaru, 1989; Mangan, Cashman & Newman, 1993) without any oxide mobilization. Since actual observed vesicle fillings are silicate minerals, chemical element transfers from basalt to geodes must have taken place. Geochemical mass balances indicate that SiO_2 was the only mobile component, whereas other major elements do not show any significant mass transfers from rock to geode (Fig. 4a). This behaviour does not agree with the currently calculated mass balances for rock weathering or hydrothermal alteration, which typically show important Ca, Na and Mg release from rock to fissure through fluid circulation (White, 1995). Moreover, the petrographical and mineralogical study of the geodes and their massive hosting basalt has shown that (1) the geodic cavities always formed in massive basalt, out of possible fluid circulation pathways, (2) the secondary mineral assemblages in the geodes and in the enclosing massive basalt were very different, with saponite + chalcedony + calcite + quartz + amethyst in geodes and celadonite in the basalt, (3) the siliceous geode infillings exhibited wall-layering zonations which characterize high-temperature deposits from supercritical hydrous fluids, as opposed to horizontally layered habits which are more common for low-temperature chalcedony (Flörke *et al.* 1982). These particular features, together with fluid inclusion and geochemical data, rule out weathering or fissural hydrothermal alteration as possible origins for silica transfers. They are better understood when considering the geode and its host-basalt as a closed system where high temperature authigenic fluids react with basalt to produce an alteration halo around the geode (most elements are trapped in secondary minerals of the alteration halo) with migration of excess silica towards the geodic cavity. In these conditions, the driving force for chemical element transfers is the pressure gradient of water vapour between vesicles/geodes and basalt which induces the chemical diffusion process and thus the formation of chemical potential gradients in relation with the magma cooling. The vesiculation processes (bubble nucleation, growth and ascent) stop when the temperature drops to about 1000 °C because of increasing magma viscosity (Goff, 1996). The geodic cavities thus stop forming at about 1000 °C, whereas amethyst crystallizes at about 250 °C. The cooling from 1000 °C to 250 °C will decompress the H_2O-rich gas in the geode with the formation of pressure and chemical gradients (Anderson *et al.* 1984). These gradients allow the migration of residual, differentiated hot fluids, from the diktytaxitic sites in basalt (Walker, 1989) to the geode, with synchronous formation of alteration halo in the surrounding host-rock.

The part played by chemical diffusion in the geodic silica crystallizations can be estimated from the geochemical mass balances which were calculated in the geode levels as a function of the distance to the geode (Fig. 4a). It was observed that silica was the major mobile component with an increasing mass release from rock to the geode (7.53 g SiO_2 released

https://doi.org/10.1017/S0016756807003457 Published online by Cambridge University Press

per 100 g of basalt at the contact with the geode). The mass balances were calculated for 100 g of basalt with a density of 2.89 g/cm^3, that is, a rock unit volume of 34.60 cm^3 with a cubic edge of 3.26 cm. Spherical geodes were first simulated with various silica rim thicknesses and various geode radii. The amount of SiO_2 (d = 2.65 g/cm^3) needed for each silica rim thickness in each geode was then calculated and compared to the SiO_2 released by successive spherical rims of basalt using an increment of 3.26 cm along the SiO_2 curve given in Figure 4a. The amount of SiO_2 released by these successive basalt rims was then cumulated until sufficient to account for the given geodic silica rim crystallization. From the geochemical modelling, one can calculate, for a given geode radius, the thickness of the basalt rim, the alteration of which (SiO_2 release) produced the given silica rim (Fig. 4b). This geochemical modelling, however, has to be checked with the observed amethyst quartz geode features, as described by the image analysis data of the 106 exposed quartz amethyst geodes. The maximum radius (53.30 cm) and the maximum silica rim thickness (11.30 cm) give a maximum geode infilling of 49 %. These values, when plotted in Figure 4b, indicate that this 'maximum' geode requires an altered basalt rim with 35 cm thickness in order to provide sufficient SiO_2 for amethyst crystallizations.

The image analysis data of the mining galleries, that is, geode radii and distances between neighbouring geodes, were used to model the altered basalt rim surrounding each geode. Calculations were made considering, respectively, 100 % geode infilling to maximize the alteration halo, and 49 % infilling to match the maximum infilling observed in the exposed geodes. The results are given in Figure 4c, where altered basalt rim thicknesses are plotted versus distances to the neighbouring geodes. For the two infilling values, it appears that the sum of the thicknesses of the altered basalt rims surrounding two neighbouring geodes is always smaller than the distance observed between these two geodes. Our model is in good agreement with the geode observations in the mining galleries: two neighbouring geodes with 53.30 cm radius are 78 cm apart. Their mean silica rims are 11.30 cm thick, which requires a minimum altered basalt rim of 35 cm. This indirectly indicates (1) that the amount of silica released by the basalt is always sufficient to account for the internal silica rims of the geodes without interferring with their neighbours and (2) that no external silica supply is needed for the geodic silica crystallizations.

A possible explanation of the mechanism leading to the transfer of silica from basalt to geodes could be the pre-existence of geodic cavities responsible for the development of chemical gradients during the crystallization of minerals in the host basaltic rock and associated water release. This water will diffuse towards geodic voids (depressurized domains) and promote highly reactive glass alteration with strong silica lixiviation. When Si-rich fluid enters the geodic cavities, pressure and temperature drastically decrease and lead to water activity decrease with demixing between water (liquid and/or vapour) and silica gel. Such a gel favours the fast crystallization of chalcedony at the beginning and amethyst at the end of the crystallization process as demonstrated by Wang & Merino (1990) and Merino, Wang & Deloule (1995). According to the SiO_2/H_2O ratio, the crystallization system may produce more or less chalcedony or amethyst. Flörke *et al.* (1982) proposed two stages for vesicle infillings: (1) in the early stages of lava cooling, supercritical differentiated fluids with low viscosity and a low degree of siliceous polymerization can enter the geodes and lead to the rapid deposit of stressed microcrystalline wall-layered chalcedony; (2) further cooling and pressure decrease will cause silica-bearing fluids with low supersaturation and a high degree of polymerization to infiltrate the geode with fine-grained quartz and amethyst crystallization, down to 250 °C. However, in our study, no evidence allows us to decide if the successive crystallizations of chalcedony and amethyst are due to only one fluid with decreasing SiO_2/H_2O ratio, or two fluids with respectively high and low SiO_2/H_2O ratios.

6. Conclusion

This study demonstrates that the siliceous minerals observed in the geodes of the Triz quarry (Ametista do Sul, Brazil) have crystallized in closed geochemical systems, within the 300 °C to 200 °C temperature range, from post-magmatic fluids. These fluids were probably locally driven from the diktytaxitic sites of the surrounding host basalt to the geodic cavities by a filter pressing mechanism. These fluids interacted with the host-rock to produce a wall-layering alteration rim around the geodes. This alteration rim trapped most elements in secondary crystallizations. Excess silica entered the geodic cavity and crystallized in the form of chalcedony, fine-grained quartz and amethyst, without any contribution from an extraneous source.

Acknowledgements. The authors would like to acknowledge Dr Honnorez and Dr Merino for their thorough reviews and helpful comments.

References

ALBAREDE, F. & PROVOST, A. 1977. Petrological and geochemical mass balance equations: an algorithm for least-square fitting and general error analysis. *Computers and Geosciences* **3**, 309–26.

ANDERSON, A. T. 1975. Some basaltic and andesitic gases. *Reviews of Geophysics and Space Physics* **13**, 37–55.

ANDERSON, A. T. JR, SWIHART, G. H., ARTIOLI, G. & GEIGER, C. A. 1984. Segregation vesicles, gas filter-pressing, and igneous differentiation. *Journal of Geology* **92**, 55–72.

https://doi.org/10.1017/S0016756807003457 Published online by Cambridge University Press

BALITSKY, V. S. 1978. Les conditions de formation des améthystes et leur croissance artificielle. *Bulletin de Minéralogie* **101**, 383–6.

BELLIENI, G., COMIN-CHIARAMONTI, P., ERNESTO, M., MELFI, A. J., PACCA, I. G. & PICCIRILLO, E. M. 1984. Flood basalt to rhyolite suites in the southern Paraná plateau (Brazil): paleomagnetism, petrogenesis and geodynamic implications. *Journal of Petrology* **25**, 579–618.

BIDDLE, D. L., CHITTLEBOROUGH, D. J. & FITZPATRICK, R. W. 1998. An algorithm to model mass balances quantitatively. *Computers and Geosciences* **24**, 77–82.

BORGET, J. N. 1985. *Contribution à l'étude de la genèse des minéralisations siliceuses associées aux roches basaltiques du nord-ouest de l'Uruguay*. Published Ph.D. thesis, University of Clermont-Ferrand, France.

BOSSI, J. & CAGGIANO, W. 1974. Contribuicion a la geologia de amatista del Departamento de Artigas (Uruguai). *SBG, Congresso Brasileiro de Geologia* **28**, 301–18.

BRIMHALL, G. H. & DIETRICH, W. E. 1987. Constitutive mass balance relations between chemical composition, volume, density, porosity, and strain in metasomatic hydrochemical systems: results on weathering and pedogenesis. *Geochimica et Cosmochimica Acta* **51**, 567–87.

CASHMAN, K. V. & MARSH, B. 1988. Crystal size distribution (CSD) in rocks and the kinetics and dynamics of crystallization: II. Makaopuhi lava lake. *Contributions to Mineralogy and Petrology* **99**, 292–305.

DUARTE, L. D. C., HARTMANN, L. A. & VASCONCELLOS, M. A. Z. 2005. Epigenetic geode formation in the world-class amethyst deposits of the southern Paraná basaltic province. *I Simpósio Brasileiro de Metalogenia, 2005, Gramado. CD-ROM*. Porto Alegre. Sociedade Brasileira de Geologia, 2005.

FALLICK, A. E., JOCELYN, J., DONNELLY, T., GUY, M. & BEHAN, C. 1985. Origin of agates in volcanic rocks in Scotland. *Nature* **313**, 672–74.

FALLICK, A. E., JOCELYN, J. & HAMILTON, P. J. 1987. Oxygen and hydrogen stable isotope systematics in Brasilian agates. In *Geochemistry and Mineral Formation in the Earth Surface* (eds R. Rodriguez-Clemente & Y. Tardy), p. 117. *Consejo Superior de Investigaciónes Scientificas, Madrid* **99**.

FLÖRKE, O. W. 1972. Transport and deposition of SiO_2 with H_2O under supercritical conditions. *Kristallographie und Technik* **7**, 159–66.

FLÖRKE, O. W., KÖHLER-HERBERTZ, B., LANGER, K. & TÖNGES, I. 1982. Water in microcrystalline quartz of volcanic origin: agates. *Contributions to Mineralogy and Petrology* **80**, 324–33.

GATTER, I. 1987. Fluid inclusion studies in the polymetallic ores of Gjöngyösoroszi (North Hungary) – Spatial and temporal evolution of ore-forming fluids. *Chemical Geology* **61**, 169–81.

GILG, H. A., MORTEANI, G., KOSTITSYN, Y., PREINFALK, C., GATTER, I. & STRIEDER, A. J. 2003. Genesis of amethyst geodes in basaltic rocks of the Serra Geral Formation (Ametista do Sul, Rio Grande do Sul, Brazil): a fluid inclusion, REE, oxygen, carbon, and Sr isotope study on basalt, quartz, and calcite. *Mineralium Deposita* **38**, 1009–25.

GOFF, F. 1996. Vesicle cylinders in vapour-differentiated basalt flows. *Journal of Volcanology and Geothermal Research* **71**, 167–85.

GOMES, M. E. B., MEXIAS, A. S., SCOPEL, R., BONGIOLO, E. M., FORMOSO, M. L. L. & MILARA, T. 2005. Volcanic sequence of the amethyst district in South Paraná Province, Rio Grande do Sul, Brazil: flow emplacement mechanisms and geodes formation. *I Simpósio Brasileiro de Metalogenia, 2005, Gramado*. CD-ROM. Porto Alegre. Sociedade Brasileira de Geologia, 2005.

GRANT, J. A. 1986. The isocon diagram – a simple solution to Gresen's equation for metasomatic alteration. *Economic Geology* **81**, 1976–82.

GRAETSCH, H., FLÖRKE, O. W. & MIEHE, G. 1985. The nature of water in chalcedony and opal-C from Brazilian agate geodes. *Physics and Chemistry of Minerals* **12**, 300–6.

GRESENS, R. L. 1967. Composition-volume relationships of metasomatism. *Chemical Geology* **2**, 47–65.

HARRIS, C. 1989. Oxygen isotope zonation of agates from Karoo volcanics of the Skeleton Coast, Namibia. *American Mineralogist* **74**, 476–81.

LANSON, B. & BESSON, G. 1992. Characterization of the end of smectite to illite transformation: decomposition of X-ray patterns. *Clays and Clay Minerals* **40**, 40–52.

LONG, P. E. & WOOD, B. J. 1986. Structures, textures, and cooling histories of Columbia River basalt flows. *Geological Society of America Bulletin* **97**, 1144–55.

MACLEAN, W. H. 1990. Mass change calculations in altered rock series. *Mineralium Deposita* **25**, 44–9.

MANGAN, M. T., CASHMAN, K. V. & NEWMAN, S. 1993. Vesiculation of basaltic magma during eruption. *Geology* **21**, 157–60.

MERINO, E., WANG, Y. & DELOULE, E. 1995. Genesis of agates in flood basalts: Twisting of chalcedony fibers and trace-element geochemistry. *American Journal of Science* **295**, 1156–76.

MEUNIER, A., FORMOSO, M. L. L., PATRIER, P. & CHIES, J. O. 1988. Alteration hydrothermale de roches volcaniques liées à la genèse des améthystes – Bassin du Paraná – Sud du Brésil. *Geochimica Brasiliensis* **2**, 127–42.

MONTANA, J. R. & BOSSI, J. 1993. Neuvos datos para prospeccion de ametistas en geodas basalticas. Ejemplo en Curtinas (Tacuarembo, Uruguay). *Congresso Geologia Economica de Cordoba, Argentina*, 372–83.

PEATE, D. W., HAWKESWORTH, C. J. & MANTOVANI, M. 1992. Chemical stratigraphy of the Paraná lavas (South America): classification of magma types and their spatial distribution. *Bulletin of Volcanology* **55**, 119–39.

POTDEVIN, J. L. 1993. Gresens 92: a simple Macintosh program of the Gresens method. *Computers and Geosciences* **19**, 1229–38.

POTTER, R. W. II, CLYNNE, M. A. & BROWN, D. L. 1978. Freezing point depression of aqueous sodium chloride solutions. *Economic Geology* **73**, 284–5.

PROUST, D. & FONTAINE, C. 2007. Amethyst-bearing lava flows in the Paraná Basin (Rio Grande do Sul, Brazil): cooling, vesiculation and formation of the geodic cavities. *Geological Magazine* **144**, 53–65.

ROBINSON, R. W. & NORMAN, D. I. 1984. Mineralogy and fluid inclusion study of the Southern Amethyst vein system, Creede Mining District, Colorado. *Economic Geology* **79**, 439–47.

ROEDDER, E. 1981. Origin of fluid inclusions and changes that occur after trapping. In *Short course in fluid inclusions: application to petrology* (eds L. S. Hollister & M. L. Crawford), pp. 101–32. Mineralogical Association of Canada.

ROEDDER, E. 1984. The origin of inclusions. In *Fluid Inclusions* (ed. P. H. Ribbe), pp. 11–45. *Reviews in Mineralogy* **12**. Mineralogical Society of America.

SPARKS, R. S. J. 1978. The dynamics of bubble formation and growth in magmas: a review and analysis. *Journal of Volcanology and Geothermal Research* **3**, 1–37.

STURM, R. 2003. SHEARCALC – a computer program for the calculation of volume change and mass transfer in a ductile shear zone. *Computers and Geosciences* **29**, 961–9.

SUNAGAWA, I. & OHTA, E. 1976. Mechanism of formation of chalcedony. *Science Report Tohuku University* **13**, 131–46.

TANIGUCHI, H. 1988. Surface tension of melts in the system $CaMgSi_2O_6$–$CaAl_2Si_2O_8$ and its structural significance. *Contributions to Mineralogy and Petrology* **100**, 484–9.

TORAMARU, A. 1989. Vesiculation process and bubble size distributions in ascending magmas with constant velocities. *Journal of Geophysical Research* **94**, 17523–42.

TORAMARU, A. 1995. Numerical study of nucleation and growth of bubbles in viscous magmas. *Journal of Geophysical Research* **100**, 1913–31.

WALKER, G. P. L. 1989. Spongy pahoehoe in Hawaii: a study of vesicle-distribution patterns in basalt and their significance. *Bulletin of Volcanology* **51**, 199–209.

WANG, Y. & MERINO, E. 1990. Self-organizational origin of agate: Banding, fiber twisting, composition, and dynamic crystallization model. *Geochimica et Cosmochimica Acta* **54**, 1627–38.

WHITE, A. F. 1995. Chemical weathering rates of silicate minerals in soils. In *Chemical weathering rates of silicate minerals* (eds A. F. White & S. L. Brantley), pp. 407–61. *Reviews in Mineralogy* **31**. Mineralogical Society of America.

https://doi.org/10.1017/S0016756807003457 Published online by Cambridge University Press